Journal of Materials Chemistry B

ROYAL SOCIETY OF CHEMISTRY

PAPER

View Article Online
View Journal

Check for updates

Cite this: DOI: 10.1039/d6tb00081a

Blue light-activated berberine–gentamicin combination breaks down biofilms in diabetic foot ulcers

Ariana S.C. Gonçalves, [ab] Miguel M. Leitão, [ac] Manuel Simões [ad] and Anabela Borges *[ad]

Diabetic foot ulcers (DFUs) represent a significant global burden, associated with high morbidity and increased mortality. More than half of DFUs become infected by polymicrobial communities, in which *Pseudomonas aeruginosa* and *Staphylococcus aureus* form resilient biofilms. Antimicrobial photodynamic inactivation (aPDI) using blue light is promising, its efficacy against polymicrobial biofilms remains suboptimal in infected DFUs. This study evaluated, for the first time, the activity of a berberine–gentamicin (Ber–Gen) combination under blue light photoactivation against dual-species *P. aeruginosa* MJMC568-A and *S. aureus* MJMC568-B biofilms, both isolated from a DFU patient. First, the minimum biofilm inhibitory concentration (MBIC) and minimum biofilm eradication concentration (MBEC) for each agent against pre-formed dual-species biofilms were determined. Ber and Gen alone did not reach MBIC or MBEC at concentrations <2000 μg mL^{-1}, but in combination, MBIC values decreased two-fold to 1000 μg mL^{-1} for Ber and 1024 μg mL^{-1} for Gen. The combinatorial effect was assessed by checkerboard (CKB), with Ber–Gen resulting in a synergistic effect for MBIC values. The optimised concentrations from CKB were tested under one, two, and three irradiation cycles (with a 24 h interval between irradiation cycles) of blue light at 30 mW cm^{-2} for 10 min *per* cycle (18 J cm^{-2}). Antibiofilm activity was quantitatively assessed by biomass (crystal violet), metabolic activity (alamar blue), and culturability (colony-forming unit (CFU cm^{-2}) counts). Photoactivated Ber–Gen produced strong reductions in biomass, metabolic activity, and culturability after one cycle (≈50%, ≈70%, and ≈5 log CFU cm^{-2}, respectively), near-complete eradication after two cycles (≈60%, ≈80%, and ≈6 log CFU cm^{-2}, respectively), and a further effect after three cycles (≈90%, ≈95%, and ≈10 log CFU cm^{-2}, respectively). Regrowth assays showed full recovery after one cycle, about half recovery after two, and less than 10% recovery after three cycles. Mechanistic assays on the antibiofilm effect included measurement of reactive oxygen species (ROS) by fluorometry, membrane integrity by flow cytometry and confocal microscopy, matrix components by confocal microscopy, spectrophotometric and fluorometric assays, and architecture by optical coherence tomography. Biofilm structure was markedly disrupted, with strong reductions in thickness, extracellular matrix components such as proteins, polysaccharides, and eDNA. These structural changes coincided with a decrease in biofilm cells' membrane integrity and increased ROS production. Overall, Ber–Gen-mediated blue light aPDI exhibits strong activity against dual-species biofilms of *P. aeruginosa* and *S. aureus*.

Open Access Article. Published on 07 April 2026. Downloaded on 4/8/2026 2:33:27 PM.
This article is licensed under a Creative Commons Attribution 3.0 Unported Licence.

Received 9th January 2026,
Accepted 22nd March 2026

DOI: 10.1039/d6tb00081a

rsc.li/materials-b

1 Introduction

Currently, chronic wounds are a major health problem worldwide, affecting patients' health and quality of life.[1] This health condition occurs when the repair process fails to restore skin anatomical and functional integrity after three months.[2] Chronic wounds mainly affect adults and result from complications such as venous insufficiency, pressure ulcers, arterial insufficiency, neuropathies, and diabetes.[3] Among diabetic patients, an estimated 18.6 million individuals worldwide

[a] *LEPABE, ALiCE, Faculty of Engineering, University of Porto, Rua Dr Roberto Frias, s/n, 4200-465 Porto, Portugal. E-mail: apborges@fe.up.pt*
[b] *Environmental Health Department, Portuguese National Health Institute Doutor Ricardo Jorge, Porto, Portugal*
[c] *CIQUP-IMS-Department of Chemistry and Biochemistry, Faculty of Sciences, University of Porto, Rua do Campo Alegre, 4169-007, Porto, Portugal*
[d] *DEQB-Department of Chemical and Biological Engineering, Faculty of Engineering, University of Porto, Rua Dr Roberto Frias, s/n, 4200-465 Porto, Portugal*

Open Access Article. Published on 07 April 2026. Downloaded on 4/8/2026 2:33:27 PM.
This article is licensed under a Creative Commons Attribution 3.0 Unported Licence.

suffer from diabetic foot ulcers (DFUs).[4] The five-year mortality rate for DFUs is about 30%, increasing to over 70% in cases involving major amputation.[5] This worsening scenario is largely due to the high susceptibility of DFUs to infection, with around 60% becoming infected and about 20% progressing to moderate or severe infections, often leading to lower limb amputation.[6] Treatment is further complicated by the frequent colonisation of DFUs by polymicrobial biofilms.[7] In particular, biofilms are frequently found in DFUs, with prevalence rates approaching 70%.[8] When bacteria form biofilms, they become more recalcitrant, which protects them from both antibiotic treatment and the host immune response.[9] Consequently, biofilms on DFUs may be responsible for delayed healing and the subsequent chronicity of the infection.[7] *Pseudomonas aeruginosa* and methicillin-resistant *Staphylococcus aureus* (MRSA) are among the pathogens most frequently isolated from DFUs.[10] Notably, dual-species *P. aeruginosa* and *S. aureus* biofilms exhibit higher virulence than either single-species biofilm, making the treatment of DFUs particularly challenging.[11] In particular, co-infection with *P. aeruginosa* and *S. aureus* promotes the establishment of a pathogenic consortium that sustains chronic infection.[12] Interactions between these species promote the formation of polymicrobial biofilms and enhance antimicrobial tolerance, reported to increase by up to 50% in mixed biofilms.[13] Moreover, these interactions enhance the production of virulence factors (*e.g.*, exotoxin A, elastases, and pyocyanin from *P. aeruginosa*, and α-toxin and hemolysins from *S. aureus)* and sustain a prolonged inflammatory response, leading to increased host tissue damage and delayed wound healing.[11] Indeed, biofilms can also hijack host immunity, as ineffective immune cell clearance leads to persistent inflammation and excessive ROS production, which damages surrounding tissue and generates nutrients that further sustain biofilm growth.[14]

Given the low healing outcomes associated with DFUs, therapeutic strategies must address both infection control and tissue regeneration.[15] Among emerging approaches, blue light has been reported as a promising adjuvant therapy.[16] Operating within the 400–470 nm wavelength range, which is generally considered safe, it has attracted interest not only for its antimicrobial properties but also for its effects on host tissue.[17] It has been demonstrated that doses up to 40 J cm^{-2} can modulate cellular metabolism and stimulate the proliferation of host cells.[18] Additionally, blue light has been linked to antimicrobial activity due to the excitation of intracellular porphyrins, resulting in the production of reactive oxygen species (ROS).[19] These properties have resulted in the use of blue light in antimicrobial photodynamic inactivation (aPDI).[20] While blue light alone can generate ROS, combining it with exogenous photosensitisers (PSs) significantly enhances this effect, providing a more effective strategy against DFUs.[17] Among the various classes of PSs, natural compounds are promising candidates for aPDI directed for DFUs treatment due to their lower toxicity.[21] One notable example is berberine (Ber), an isoquinoline alkaloid isolated from medicinal plants such as *Hydrastis canadensis*, *Berberis aristata*, *Coptis chinensis*, and *Coptis rhizome*.[22] In addition to its photosensitising activity, Ber has long been recognised as a multipotent therapeutic agent, with reported clinical applications in gastroenteritis, abdominal pain, as well as antimicrobial, antidiabetic, and anti-inflammatory effects.[23] Importantly, the use of PSs with intrinsic antimicrobial activity further enhances aPDI, increasing bacterial damage and strengthening ROS-mediated effects.[24] Ber exemplifies this dual action, being a phytochemical with multi-target properties, capable of interacting with negatively charged bacterial membrane components, intercalating into DNA, and promoting oxidative stress even without light.[20] In addition, Ber has an absorption peak that overlaps with the emission spectrum of blue light, making it a particularly effective PS for aPDI in DFUs treatment.[17]

In fact, aPDI is an innovative and promising strategy for managing DFUs, due to its combined healing and antimicrobial effects.[25] ROS generated during aPDI are a powerful tool against bacteria due to their multi-target activity, including oxidative damage to cell membranes and walls, impairment of protein synthesis, and induction of DNA mutations.[24] This broad mechanism of action also reduces the likelihood of antimicrobial resistance compared with conventional therapies.[17] However, evidence from clinical trials remains limited, and only a few studies have investigated the specific role of aPDI in DFU treatment.[25] The rapid therapeutic action of aPDI is particularly valuable in chronic DFUs at risk of progressing to sepsis, where treatment time is critical.[24] However, when used as a standalone approach, aPDI may have significant limitations. The short lifetime (≈3.5 μs) and limited diffusion distance (≈100 nm in aqueous solution) of ROS can restrict their efficacy, contributing to infection recurrence.[17] Furthermore, bacterial defence mechanisms, such as the production of superoxide dismutase and catalase by *P. aeruginosa*, can neutralise ROS and result in incomplete inactivation.[26] To address these challenges, several strategies have been explored to enhance aPDI efficacy. One promising approach is combining aPDI with antibiotics, which has been proposed as a way to overcome both antibiotic recalcitrance and the intrinsic limitations of aPDI.[24] This dual strategy may act synergistically by disrupting biofilm structure, increasing uptake of PSs and antibiotics, reducing bacterial antioxidant defences, and potentiating the effects of ROS, antibiotics, and the intrinsic antimicrobial activity of PSs.[27]

Based on the existing knowledge gaps, this study investigated, for the first time, the activity of blue light aPDI using a Ber–gentamicin (Ber–Gen) combination against dual-species *P. aeruginosa* MJMC5686A and *S. aureus* MJMC5686B biofilms. *P. aeruginosa* MJMC5686A is a multidrug-resistant strain and *S. aureus* MJMC5686B is an MRSA strain, both isolated from a patient with a DFU.[17] Ber was selected for its antimicrobial and photosensitising properties, while Gen was chosen for its clinical relevance in topical DFU treatment and its activity against both Gram-negative and Gram-positive bacteria.[17] The potential synergistic activity of Ber and Gen against dual-species biofilms was first assessed by the checkerboard (CKB) assay. To better simulate DFU treatment, multiple irradiation cycles were performed to evaluate their ability to eradicate preformed biofilms. In addition, biofilm regrowth was monitored

 This journal is © The Royal Society of Chemistry 2026

Open Access Article. Published on 07 April 2026. Downloaded on 4/8/2026 2:33:27 PM. This article is licensed under a Creative Commons Attribution 3.0 Unported Licence.

over 72 h post-treatment to assess the efficacy over time of the therapeutic effect. Finally, the mechanistic antibiofilm mode of action was explored by analysing biofilm three-dimensional (3D) architecture, extracellular polymeric substances (EPS) composition (proteins, polysaccharides, and extracellular DNA (eDNA)), bacterial membrane integrity, and ROS production.

2. Materials and methods

2.1. Bacterial strains and culture conditions

The clinical isolates *P. aeruginosa* MJMC568-A and *S. aureus* MJMC568-B were originally obtained from a patient with a DFU during a consultation at Centro Hospitalar de Trás-os-Montes e Alto Douro (Vila Real, Portugal) and are currently preserved in the microbial collection of the University of Trás-os-Montes and Alto Douro (UTAD). The isolates were used in this study in accordance with institutional guidelines for research purposes. Both strains were preserved at −80 °C in Tryptic Soy Broth (TSB; Millipore, Darmstadt, Germany) supplemented with 30% (v/v) glycerol. Prior to experimental assays, the isolates were subcultured on Tryptic Soy Agar (TSA; Millipore, Darmstadt, Germany). For testing, bacterial suspensions were prepared by overnight growth (16–18 h) in TSB at 37 °C with constant agitation (150 rpm; AGITORB 200, Aralab, Rio de Mouro, Portugal). These isolates have previously been employed as reference models in antimicrobial investigations involving phytochemicals and antibiotics.[17]

2.2. Antibiotic and photosensitiser preparation

The antibiotic Gen was acquired as a pure compound (AppliChem, Darmstadt, Germany; Fig. 1A). This antibiotic was selected due to its clinical relevance in the management of infections caused by both *P. aeruginosa* and *S. aureus*, particularly in topical therapies.[17] Stock solutions were prepared in sterile distilled water (dH_2O) following the guidelines of the Clinical and Laboratory Standards Institute (CLSI) and stored at −20 °C until further use. The phytochemical Ber was also obtained as a pure compound (Cayman Chemical Company, Michigan, USA; Fig. 1A and B) and employed as PS.[17] Ber stock solutions were prepared in dimethyl sulfoxide (DMSO, 100%; VWR, Belgium) and stored at −20 °C in the dark. The final concentration of DMSO in bacterial suspensions never exceeded 5% (v/v).

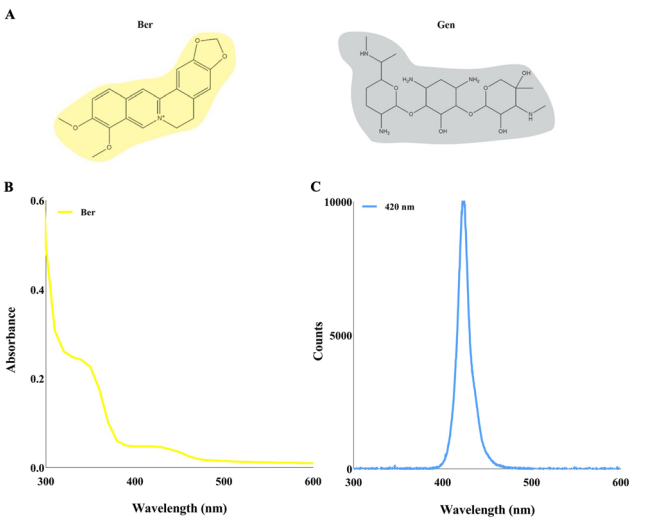

Fig. 1 Spectral and structural characterization of Ber and blue light LED. (A) Chemical structure of Ber and Gen (obtained from ChemDraw Pro 8.0). (B) UV-vis absorption spectra of Ber. (C) Emission spectrum of 420 nm LED.

2.3. aPDI parameters

The aPDI assays were performed using custom-built blue light-emitting diode (LED) devices (420 nm). For experiments conducted in 96-well plates, a system containing 40 LEDs was used, with each diode aligned to illuminate a single well, ensuring localized and uniform exposure. For assays performed in 24-well plates, a similar device was employed, consisting of 24 blue LEDs mounted in a 24-well template with equivalent optical characteristics. In both devices, all LEDs were calibrated to guarantee consistent irradiance across wells.

The power density (W cm^{-2}) of each LED device was determined using eqn (1) and (2):

$$40\ \text{LEDs device: } E_e = 0.0202 \times I_{elec} + 0.00046 \quad (1)$$

$$24\ \text{LEDs device: } E_e = 0.0630 \times I_{elec} + 0.00569 \quad (2)$$

where E_e is the power density (W cm^{-2}) and I_{elec} is the electrical current of each device LED (A).

An electric current of 1.5 and 0.4 was chosen for 40 and 24 LED devices, respectively, resulting in a power density of 30 mW cm^{-2}. The light dose (J cm^{-2}) was calculated by multiplying the power density by irradiation time (in seconds). For both LED devices, the irradiation time was 10 min, corresponding to a light dose of 18 J cm^{-2} (Fig. 1C). This blue light dose was selected based on irradiation parameters previously optimised in our previous study, where different conditions were evaluated to determine the most effective blue light settings.[17]

2.4. Biofilm assays

2.4.1. Biofilm eradication

2.4.1.1. Dual-species biofilm formation. Dual-species biofilms were formed according to Afonso *et al.*,[28] with minor modifications. *P. aeruginosa* MJMC568-A and *S. aureus* MJMC568-B were grown overnight in TSB at 37 °C and 150 rpm. The optical density (OD) of each culture was adjusted to 0.04 ± 0.002 (corresponding to 10^7 colony-forming units (CFU mL^{-1}) for both clinical strains) at 620 nm, and equal volumes of both suspensions were mixed at a 1 : 1 ratio. For assays performed in 96-well plates (Orange Scientific, Braine-l'Alleud, Belgium), 200 µL of the mixed bacterial suspension was added per well, whereas 1 mL was dispensed into each well of 24-well plates (Orange Scientific, Braine-l'Alleud, Belgium). Plates were incubated at 37 °C with agitation (150 rpm) for 24 h to allow biofilm formation.

2.4.1.2. Minimum biofilm inhibitory and eradication concentration. The minimum biofilm inhibitory concentration (MBIC)

Open Access Article. Published on 07 April 2026. Downloaded on 4/8/2026 2:33:27 PM. This article is licensed under a Creative Commons Attribution 3.0 Unported Licence.

of Ber and Gen against pre-formed dual-species biofilms was determined according to Gonçalves *et al.*,[17] using a modified broth microdilution assay. Briefly, the medium of pre-formed biofilms was removed and replaced with 190 μL of fresh TSB supplemented with 10 μL of Ber or 10 μL of Gen at different concentrations (2000–15.53 μg mL^{-1} for Ber and 2048–16 μg mL^{-1} for Gen). The antimicrobial solutions account for no more than 5% (v/v) of the final volume. Negative controls included wells containing 5% DMSO or biofilms without Ber or Gen. Absorbance at 620 nm was recorded immediately after treatment (t = 0 h) and after 24 h of incubation at 37 °C and 150 rpm using a microplate reader (Synergy HT, Biotek, Winooski, VT, USA). The MBIC was defined as the lowest concentration that stopped any increase in OD compared to the initial reading (t = 0 h), indicating inhibition of biofilm growth.

For the determination of the minimum biofilm eradication concentration (MBEC), 10 μL of the well contents corresponding to concentrations of the compound equal to or higher than the MBIC were collected and plated on TSA and incubated at 37 °C for 24 h. The MBEC was defined as the lowest concentration at which no visible growth were detected after 24 h.

2.4.1.3. Ber–Gen combined effect. The CKB assay was employed to evaluate the combined activity of Ber and Gen against pre-formed dual-species biofilms, based on Gonçalves *et al.*,[17] with some modifications. Briefly, the old medium in each well was replaced with 180 μL of fresh TSB, 10 μL of Ber, and 10 μL of Gen at different concentrations. Both compounds were tested across a concentration range corresponding to 1/64 to 1× MBEC. The final volume of Ber and Gen solutions did not exceed 10% (v/v) of the total well volume. Negative controls consisted of wells containing 5% DMSO or biofilms without Ber or Gen. Plates were incubated at 37 °C under agitation (150 rpm) in the dark for 24 h. After incubation, the MBIC and MBEC for each combination were determined as described in Section 2.4.2.2.

In addition, the interactions between Ber and Gen were evaluated using the fractional inhibitory concentration index (FIC_I) model for MBIC and MBEC values, expressed as follows in eqn (3) and (4):

$$FIC_I\ (BMIC) = FIC_{Ber} + FIC_{Gen} \quad (3)$$

$$FIC_I(BMIC) = \frac{MBIC\ Ber\ in\ combination}{MBIC\ Ber} + \frac{MBIC\ Gen\ in\ combination}{MBIC\ Gen}$$

$$FIC_I\ (BMEC) = FIC_{Ber} + FIC_{Gen} \quad (4)$$

$$FIC_I(BMEC) = \frac{MBEC\ Ber\ in\ combination}{MBEC\ Ber} + \frac{MBEC\ Gen\ in\ combination}{MBEC\ Gen}$$

The FIC_I was interpreted according to standard criteria,[29] with interactions classified as follows: synergistic ($FIC_I \leq 0.5$), additive ($0.5 < FIC_I < 1$), indifferent ($1 \leq FIC_I < 4$), and antagonistic ($FIC_I > 4$).

The results were also analysed using Combenefit software (version 2.021; https://sourceforge.net/projects/combenefit/, accessed November 2025), which allows visualization of the antimicrobial interaction according to the Bliss independence model as a function of concentration.

2.4.1.4. Ber–Gen time-response curve. The time-dependent effect of the Ber–Gen combination on pre-formed dual-species biofilms was monitored by growth curve analysis at various time intervals, adapting the protocol described by Fernandes *et al.*[29] In brief, the medium of each well was substituted with 180 μL of fresh TSB to which 10 μL of Ber and 10 μL of Gen were added at the concentrations optimised in the CKB assay. Negative controls included wells containing 5% DMSO or biofilms without Ber or Gen. The OD at 620 nm was measured at the start of the experiment (t = 0 h) and subsequently at 1 h intervals for 24 h during incubation at 37 °C using a microplate reader.

The Gompertz model was applied to analyze pre-formed dual-species biofilm growth kinetics following eqn (5):

$$A(t) = A_{max} \exp\left(-\exp\left(\frac{\mu_m \exp 1}{A_{max}}(\lambda - t) + 1\right)\right) \quad (5)$$

where $A(t)$ is the OD_{620} at time t, A_{max} the OD_{620} after 24 h, μ_m the maximum specific growth rate (min^{-1}), λ the lag phase duration (min), and t the incubation time (min). GraphPad Prism version 8.0.1 (GraphPad Software, La Jolla, CA, USA) was used to perform nonlinear regression, and the quality of model fit was evaluated by the coefficient of determination (r^2).

2.4.1.5. aPDI of pre-formed dual-species biofilms. The aPDI of pre-formed dual-species biofilms after single, dual, and triple irradiation cycles using Ber–Gen combination was performed based on the method of Silva *et al.*[30] For each irradiation cycle, the old medium was replaced with 180 μL of fresh TSB, followed by the addition of 10 μL Ber and 10 μL Gen at concentrations optimised from CKB assays. Negative controls included biofilms without Ber or Gen and 5% DMSO, with and without exposure to blue light. Plates were incubated at 37 °C with shaking (150 rpm) in the dark for the optimised period determined from time-response curves, after which biofilms were irradiated with 420 nm LED light (30 mW cm^{-2}, 10 min) under a laminar-flow hood in the dark. Following irradiation, plates were further incubated in darkness for 24 h at 37 °C with shaking (150 rpm). The process was repeated over two or three consecutive irradiation cycles at 24 h intervals for the experiments involving two or three irradiation cycles. After the incubation period, biofilms were assessed for biomass, metabolic activity, and culturability, as detailed in Section 2.4.3.

2.4.2. Biofilm regrowth. To evaluate the ability to sustain biofilm eradication over time, regrowth events were assessed for each irradiation cycle using Ber–Gen combination on pre-formed dual-species biofilms, following the approach of Fernandes *et al.*[29] Regrowth was monitored at 48 and 72 h post-treatment. The culture medium in each microtiter plate was

 This journal is © The Royal Society of Chemistry 2026

Open Access Article. Published on 07 April 2026. Downloaded on 4/8/2026 2:33:27 PM. This article is licensed under a Creative Commons Attribution 3.0 Unported Licence.

replaced every 24 h with 200 μL of fresh TSB, and incubations were carried out in the dark at 37 °C with shaking at 150 rpm between medium replacements. After the incubation period, biofilms were assessed for biomass, metabolic activity, and culturability, as detailed in Section 2.4.3.

2.4.3. Quantification. After incubation, the wells were aspirated, and a sodium chloride solution (NaCl; 8.5 g L^{-1}, Avantor, VWR, Radnor, PA, USA) was applied to remove planktonic and loosely attached bacteria. To inactivate any residual antimicrobial activity, a universal neutralizing solution was added to each well and left for 15 min. This neutralizer was prepared in 0.0025 M phosphate buffer and contained 30 g L^{-1} polysorbate 80 (VWR Chemicals, Le Havre, France), 30 g L^{-1} saponin (VWR Chemicals, Leuven, Belgium), 1 g L^{-1} L-histidine (Merck, Tokyo, Japan), 3 g L^{-1} lecithin (Alfa Aesar, Karlsruhe, Germany), and 5 g L^{-1} sodium thiosulfate (Labkem, Barcelona, Spain).[17]

Biofilms obtained from eradication and regrowth assays were evaluated using three complementary approaches: culturability (expressed as CFU cm^{-2} on TSA), total biomass (determined by crystal violet staining (CV; Merck, Tokyo, Japan)), and metabolic activity (assessed using Alamar Blue (AB; Sigma-Aldrich, Germany)).

2.4.3.1. Biofilm culturable cells. The culturability of biofilm cells was evaluated following the procedure described by Borges *et al.*[31] Biofilms were detached by scraping the wells of the microtiter plates three times for 1 min each and resuspended in 200 μL of NaCl solution. The suspensions were transferred to sterile labeled microcentrifuge tubes, and serial 10-fold dilutions were prepared in NaCl. From each dilution, 10 μL was spread onto TSA plates, which were incubated at 37 °C for 24 h. Colonies were visually inspected and counted when the number of CFU ranged between 10 and 200, and results were expressed as CFU cm^{-2} of the microtiter plate, calculated according to eqn (6) and (7):

$$\text{CFU mL}^{-1} = \frac{N}{W_V \times \text{Dilution}} \quad (6)$$

where N is the number of CFU in PCA plates and W_V is the sample volume in mL.

$$\text{CFU cm}^{-2} = \frac{\text{CFU mL}^{-1} \times W_V}{W_A} \quad (7)$$

where W_V is the working volume of the well and W_A is the area of the well in cm^2.

2.4.3.2. Biomass. Biomass was quantified by CV staining following the protocol of Leitão *et al.*[32] For fixation, 250 μL of 99% ethanol (Diprolar, Odivelas, Portugal) was added to each well and incubated for 15 min. The ethanol was then removed, and the plates were air-dried for 5 min at room temperature. Subsequently, biofilms were stained with 200 μL of 1% (v/v) CV solution for 5 min. Excess dye was discarded, and the bound stain was solubilized with 200 μL of 33% (v/v) glacial acetic acid (Chem-Lab, Zedelgem, Belgium). Absorbance was recorded at 570 nm using a microplate reader, and results were expressed as percentage biomass (%Biomass), calculated according to eqn (8):

$$\%\text{Biomass} = \frac{A_T}{A_C} \times 100 \quad (8)$$

where A_C represents the absorbance value (λ = 570 nm) of untreated biofilms and A_T is the OD value (λ = 570 nm) for biofilms exposed to selected compounds.

2.4.3.3. Biofilm cells metabolic activity. The metabolic activity of biofilm cells was determined following the procedure of Borges *et al.*[31] In each well, 190 μL of fresh TSB was combined with 10 μL of AB indicator solution (0.4 mM, prepared in dH_2O). Plates were incubated in the dark at 37 °C for 1 h, after which fluorescence was recorded with a microplate reader at 570 nm excitation and 590 nm emission. Results were expressed as the percentage of biofilm cells' metabolic activity (%BCMA), calculated according to eqn (9):

$$\%\text{BCMA} = \frac{F_T}{F_C} \times 100 \quad (9)$$

where F_C represents the fluorescence intensity value of untreated biofilms and F_T is the fluorescence intensity value for biofilms exposed to selected compounds.

2.4.4. Mode of action assays

2.4.4.1. Reactive oxygen species production. Intracellular ROS levels were quantified using the fluorescent probe 2,7-dichlorodihydrofluorescein diacetate (DCF-DA; Alfa Aesar, Karlsruhe, Germany), following the procedure of Gonçalves *et al.*[20] with modifications. Biofilms were incubated with DCF-DA at 10 μM for 30 min at 37 °C in the dark under shaking (150 rpm). After incubation, the probe solution was removed, and the biofilms were gently washed with sterile NaCl solution. Fresh TSB (180 μL) supplemented with 10 μL Ber and 10 μL Gen was then added, and plates were incubated at 37 °C, 150 rpm in the dark. Irradiation was performed using a 420 nm LED light source (30 mW cm^{-2}) for 10 min. Control wells were processed in parallel without irradiation. Hydrogen peroxide (H_2O_2, 3% v/v) was used as a positive control for ROS generation.[41]

Fluorescence of oxidized DCF-DA (λ_{ex} = 488 nm, λ_{em} = 540 nm) was recorded immediately after irradiation (t = 0 h) and at 24 h using a microplate reader. DCF-DA fluorescence values were normalized to the metabolic activity (using the AB assay described in Section 2.4.4.1) of the biofilms, determined in parallel with the DCF-DA assay. The normalized ROS levels were calculated according to the eqn (10):

$$\%\text{ROS} = \frac{F_{\text{DCF-DA}}}{F_{\text{AB}}} \quad (10)$$

where $F_{\text{DCF-DA}}$ represents the fluorescence intensity value of the DCF-DA probe and F_{AB} denotes the fluorescence intensity obtained from the AB assay.

2.4.4.2. Biofilm thickness and roughness. Biofilm thickness and surface roughness after multiple irradiation cycles with the Ber–Gen combination were evaluated by optical coherence

Open Access Article. Published on 07 April 2026. Downloaded on 4/8/2026 2:33:27 PM. This article is licensed under a Creative Commons Attribution 3.0 Unported Licence.

tomography (OCT), following the procedure described by Leitão *et al.*[33] Dual-species *P. aeruginosa* and *S. aureus* biofilms were grown on transparent polystyrene coupons (1 × 1 cm), which were previously cleaned and sterilized as outlined by Gomes *et al.*[34] After 72 h, the MHB medium was gently removed, and 1 mL of NaCl solution was added to each well containing a coupon before imaging. OCT analysis was performed using a Thorlabs Ganymede spectral-domain system (Thorlabs GmbH, Dachau, Germany) with a central wavelength of 930 nm and a visualization field of 3.66 × 2.98 mm^3 in the X–Z plane (1024 × 1024 pixels). Each coupon was scanned in two-dimensional (2D) across at least six independent fields of view to ensure data reproducibility. Image processing was carried out with the Biofilm Imaging and Structure Classification Automatic Processor (BISCAP), as described by Narciso *et al.*[35] For each experimental condition, a minimum of six 2D-OCT images were acquired in every independent replicate.

2.4.4.3. Confocal laser scanning microscopy analysis. Confocal laser scanning microscopy (CLSM) was used to analyse the 3D organization of dual-species *P. aeruginosa* and *S. aureus* biofilms, focusing on the cell membrane integrity and biofilm extracellular matrix, following the protocol of Mohammed *et al.*[36] with modifications. After treatment, the TSB medium was removed, and biofilms were gently rinsed with 1 mL of sterile NaCl solution to eliminate planktonic or weakly attached cells. Coupons were then transferred to a clean plate and subjected to sequential fluorescent staining.

2.4.4.3.1. Biofilm cells distribution and membrane integrity. Bacterial cells were stained with SYTO9 and propidium iodide (PI) from the LIVE/DEAD™ BacLight™ Bacterial Viability Kit (Thermo Fisher Scientific, Waltham, MA, USA). A mixture of SYTO9 and PI (total volume 300 µL) was added to each coupon and incubated for 7 min in the dark. SYTO9-stained cells (green) represented bacterial cells with intact membranes, whereas PI-stained cells (red) indicated membrane-compromised cells. Imaging was carried out using a Leica STELLARIS 5 confocal microscope (Leica Microsystems, Wetzlar, Germany) equipped with a 63× oil immersion objective. Fluorescence detection was configured as follows:

SYTO9: excitation 488 nm, emission 500–550 nm (green channel)

PI: excitation 561 nm, emission 590–650 nm (red channel)

Z-stacks were acquired for 3D reconstruction and processed using Imaris software (Bitplane, Zürich, Switzerland), enabling visualization of the spatial distribution of intact and membrane-compromised cells within the biofilm.

2.4.4.3.2. Biofilm structure analysis. To visualise extracellular matrix components, coupons were first stained with 300 µL of SYPRO® Ruby Biofilm Matrix Stain (Thermo Fisher Scientific, Waltham, MA, USA) for 30 min at room temperature in the dark, followed by gentle rinsing with NaCl solution. For eDNA visualization, 4′,6-diamidino-2-phenylindole (DAPI; Merck, Darmstadt, Germany) was then applied at a final concentration of 1 µg mL^{-1} for 5 min in the dark, and excess stain was carefully removed before imaging. Microscopy was performed with the same CLSM system and objective. Fluorescence detection parameters were set as:

DAPI: excitation 405 nm, emission 430–470 nm (blue channel)

SYPRO® Ruby: excitation 638 nm, emission 650–700 nm (red channel)

Z-stacks were acquired and reconstructed in Imaris software, allowing simultaneous visualization of eDNA (blue) and protein-rich EPS (red) distribution within the biofilm matrix.

2.4.4.4. EPS matrix components quantification. The quantification of extracellular protein and polysaccharides from dual-species *P. aeruginosa* and *S. aureus* biofilms was performed following the protocol of Pereira *et al.*[37] Briefly, biofilm suspensions were diluted in an extraction buffer containing 0.76 g L^{-1} $Na3PO_4{\cdot}12H_2O$ (Merck, Darmstadt, Germany), 0.36 g L^{-1} $Na_2HPO_4{\cdot}H_2O$ (VWR Chemicals, Leuven, Belgium), 0.53 g L^{-1} NaCl, and 0.08 g L^{-1} KCl (VWR Chemicals, Leuven, Belgium), prepared in ultrapure H_2O. The suspensions were then mixed with Dowex® Marathon© resin (Na^+ form, strongly acidic, 20–50 mesh; Sigma-Aldrich, Germany) and incubated for 4 h at 4 °C under continuous shaking (400 rpm). Samples were then centrifuged at 3700 × *g* for 5 min to separate the EPS-containing supernatant from the cellular fraction.

Polysaccharides were determined by the phenol-sulfuric acid method using glucose as the calibration standard, according to Dubois *et al.*[38] Protein was quantified by the Bradford assay, following Harlow *et al.*,[39] with bovine serum albumin (BSA) as the reference standard. Detection limits were 0.9 µg cm^{-2} for polysaccharides and 4.5 µg cm^{-2} for proteins.

The quantification of biofilm eDNA was performed using DAPI following a modified procedure of Zatorska *et al.*[40] Briefly, biofilm suspensions were diluted in an extraction buffer consisting of 6.06 g L^{-1} Tris-HCl (Eurobio, Les Ulis, France), 3.72 g L^{-1} ethylenediamine tetraacetate (EDTA; VWR Chemicals, Leuven, Belgium), and 0.1% of polysorbate 80, adjusted to pH = 8.0 with NaOH or HCl, and prepared in ultrapure H_2O. Suspensions were vortexed for 10 min and centrifuged at 3700 × *g* for 15 min at 4 °C. The supernatant containing eDNA was carefully collected and transferred to sterile microcentrifuge tubes. Samples were then incubated with DAPI at a final concentration of 1 µg mL^{-1} for 5 min in the dark, and fluorescence was measured immediately using a microplate reader at an excitation wavelength of 355 nm and emission of 460 nm.

2.4.4.5. Biofilm cells' membrane integrity. Membrane integrity of biofilm cells was also evaluated by cytometry using PI from the Live/Dead Backlight™ Viability Kit, following the procedure of Leitão *et al.*[41] with slight modifications. After treatment, the TSB medium was carefully removed from each well and replaced with 1 mL of sterile NaCl solution to eliminate non-adherent or weakly attached cells. Coupons were then transferred into sterile tubes containing 1 mL of NaCl and vortexed for 5 min to release biofilm. From each biofilm

 This journal is © The Royal Society of Chemistry 2026

Open Access Article. Published on 07 April 2026. Downloaded on 4/8/2026 2:33:27 PM.
This article is licensed under a Creative Commons Attribution 3.0 Unported Licence.

suspension, 950 μL were mixed with 50 μL of PI (at a final concentration of 0.074 mM) and incubated for 7 min in the dark. Biofilm suspensions obtained from untreated biofilms were used as negative controls. Flow cytometry was performed on a CytoFLEX cytometer (model V0-B3-R1, Beckman Coulter, Brea, CA, USA) using the PC5.5-A channel, and data were acquired and analyzed with CytExpert software (version 2.4.0.28, Beckman Coulter).

2.5. Statistical analysis

The means and standard deviations (SDs) within samples were calculated for all conditions. Experimental data were analyzed using one-way ANOVA multiple comparisons with the statistical program GraphPad Prism 8.0.1 for Windows (GraphPad Software, La Jolla, California, USA). Statistical differences were determined for a probability level of 95% (* $P < 0.05$), 99% (** $P < 0.01$), 99.9% (*** $P < 0.001$), and 99.99% (**** $P < 0.0001$). Significant differences were also marked by letters above the bars, where *a* stands to ****, *b* to ***, *c* to **, and *d* to *. All experiments were performed in duplicate with at least three repetitions per condition.

3. Results

3.1. Activity of Ber–Gen combination against pre-formed biofilms

The MBIC and MBEC of Ber and Gen were determined against dual-species *P. aeruginosa* MJMC568-A and *S. aureus* MJMC568-B biofilms (Fig. 2A). Individually, for both compounds, no MBIC or MBEC values were found up to the maximum tested concentration (MTC = 2000 μg mL^{-1}). However, in combination, the MBIC of Ber and Gen decreased to 1000 and 1024 μg mL^{-1}, respectively. MBEC values showed no substantial reduction, resulting in 2000 μg mL^{-1} for Ber and 2048 μg mL^{-1} for Gen. These findings indicate a synergistic interaction at the MBIC level and an indifferent effect at the MBEC level (Fig. 2B). Consistently, Combenefit analysis demonstrated that synergistic interactions at the MBIC level occurred across a wide range of concentrations in dual-species biofilms (Fig. 2C and D).

The eradication potential of the Ber–Gen combination against pre-formed dual-species *P. aeruginosa* MJMC568-A and *S. aureus* MJMC568-B biofilms was assessed using Ber–Gen MBIC (1000–1024 μg mL^{-1}). To gain deeper insight into the impact of Ber, Gen, and their combination on the growth dynamics of dual-species biofilms under non-photoactivated conditions, growth curves were monitored over 24 h by absorbance measurements and fitted to the Gompertz model. The resulting parameters (A_{max}, μ_m, and λ) are presented in Table 1.

Analysis of the parameters of the Gompertz model revealed different effects of Ber, Gen, and their combination on the pre-formed dual-species *P. aeruginosa* MJMC568-A and *S. aureus* MJMC568-B biofilms (Fig. 2E). The untreated control showed the highest A_{max} (1.784) and a positive growth rate (μ_m = 0.823 min^{-1}) with a lag phase of 1.253 min. Treatment with

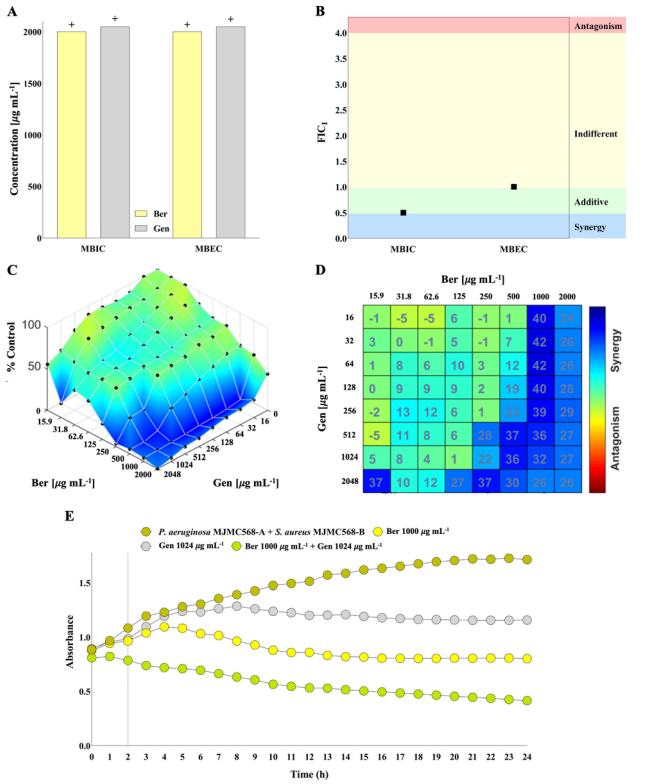

Fig. 2 Effect of Ber–Gen combination against pre-formed dual-species *P. aeruginosa* MJMC568-A and *S. aureus* MJMC568-B biofilms. (A) MBIC and MBEC values (μg mL^{-1}) of Ber and Gen tested individually (+ above the bars stands for MBIC and MBEC above the MTC). (B) FICI values for the Ber–Gen combination. Bliss synergism mapped to D–R (C) and matrix synergism plot (D) for Ber–Gen combination. (E) Growth kinetics of dual-species biofilms in the absence and presence of Ber, Gen, and Ber–Gen over 24 h.

Table 1 The Gompertz model fitting results for Ber, Gen, and Ber–Gen combination against pre-formed dual-species *P. aeruginosa* MJMC568-A and *S. aureus* MJMC568-B biofilms at different time points. Amax corresponds to OD (λ = 620 nm) after 24 h of exposure, μm is the maximum specific growth rate (min^{-1}), and λ is the lag time length (min)

	A_{max}	μ_m	λ
Control	1.784	0.823	1.253
Ber 1000	1.385	−0.105	0.952
Gen 1024	1.201	−0.341	0.821
Ber 1000 + Gen 1024	0.855	−0.073	0.022

Ber alone (1000 μg mL^{-1}) moderately reduced A_{max} (1.385) and suppressed μ_m to a negative value (−0.105 min^{-1}), while the lag phase was slightly shortened (0.952 min). Gen alone (1024 μg mL^{-1}) further reduced A_{max} (1.201), maintained a negative μ_m (− 0.341 min^{-1}), and resulted in a lag phase of 0.821 min. The Ber–Gen combination had the strongest inhibitory effect, reducing A_{max} to 0.855, almost eradicating μ_m (−0.073 min^{-1}) and drastically shortening the lag phase (λ = 0.022 min). Overall, these results indicate that Ber and Gen significantly affect the growth capacity of dual-species biofilms, with the combination exerting the strongest effect. Notably,

Open Access Article. Published on 07 April 2026. Downloaded on 4/8/2026 2:33:27 PM.
This article is licensed under a Creative Commons Attribution 3.0 Unported Licence.

growth inhibition by the Ber–Gen combination was evident as early as 2 h after incubation, suggesting that this time point may represent an appropriate drug-to-light interval for initiating blue light irradiation.

3.2. Antimicrobial photodynamic inactivation of pre-formed biofilms using the Ber–Gen combination

To evaluate the ability of blue light to potentiate the activity of the Ber–Gen combination against pre-formed dual-species *P. aeruginosa* MJMC568-A and *S. aureus* MJMC568-B biofilms, the biofilms were exposed to one, two, or three irradiation cycles (420 nm, 30 mW cm^{-2}, 18 J cm^{-2}). As shown in Fig. 3, 4, and 5, photoactivated Ber–Gen treatment markedly reduced metabolic activity, biomass, and culturability.

The application of a single cycle of blue light irradiation significantly increased the activity of the Ber–Gen combination against dual-species *P. aeruginosa* MJMC568-A and *S. aureus* MJMC568-B biofilms. After 24 h, non-photoactivated Ber or Gen alone reduced culturability by ≈2 log CFU cm^{-2} for *P. aeruginosa* and by ≈4 log CFU cm^{-2} for *S. aureus* (Fig. 3B, $P < 0.05$). Non-photoactivated Ber–Gen combination achieved an even higher reduction of ≈4 log CFU cm^{-2} in both species compared to untreated controls ($P < 0.05$). Blue light further enhanced the effect of all treatments, particularly in *S. aureus*, where complete

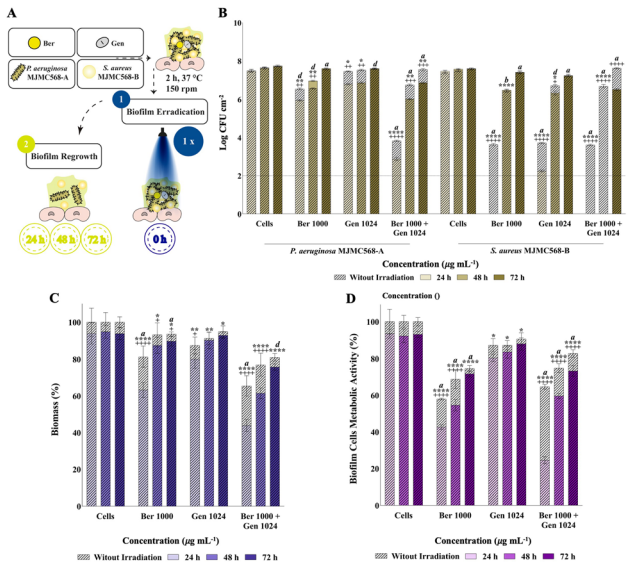

Fig. 3 Eradication of pre-formed dual-species *P. aeruginosa* MJMC568-A and *S. aureus* MJMC568-B biofilms with Ber, Gen, and their combination after one irradiation cycle. (A) Schematic representation of the experimental workflow: pre-formed dual-species biofilms were exposed to Ber, Gen, or Ber–Gen combination for 2 h at 37 °C under agitation (150 rpm), followed by blue light irradiation (420 nm, 30 mW cm^{-2}, 18 J cm^{-2}) during 10 min. Regrowth was assessed over 72 h by evaluating the culturability of *P. aeruginosa* MJMC568-A and *S. aureus* MJMC568-B, expressed as log CFU cm^{-2} (B), total biomass (C), and metabolic activity (D). Data are presented as mean ± SDs for two independent experiments with at least three replicates. Statistical analyses were performed between irradiated and non-irradiated groups (represented by the +), relative to untreated biofilm controls (represented by *), and between time points (24, 48, and 72 h), with significant differences indicated by the letters above the bars.

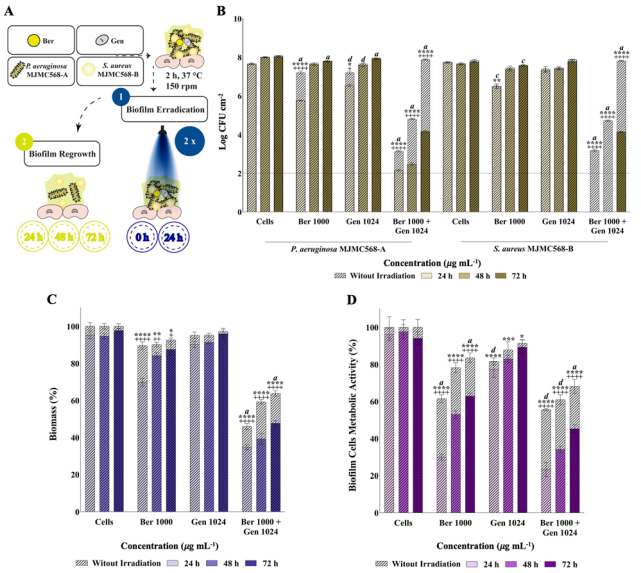

Fig. 4 Eradication of pre-formed dual-species *P. aeruginosa* MJMC568-A and *S. aureus* MJMC568-B biofilms with Ber, Gen, and their combination after two irradiation cycle. (A) Schematic representation of the experimental workflow: pre-formed dual-species biofilms were exposed to Ber, Gen, or Ber–Gen combination for 2 h at 37 °C under agitation (150 rpm), followed by blue light irradiation (420 nm, 30 mW cm^{-2}, 18 J cm^{-2}) during 10 min. Regrowth was assessed over 72 h by evaluating the culturability of *P. aeruginosa* MJMC568-A and *S. aureus* MJMC568-B, expressed as log CFU cm^{-2} (B), total biomass (C), and metabolic activity (D). Data are presented as mean ± SDs for two independent experiments with at least three replicates. Statistical analyses were performed between irradiated and non-irradiated groups (represented by the +), relative to untreated biofilm controls (represented by *), and between time points (24, 48, and 72 h), with significant differences indicated by the letters above the bars.

eradication (≈8 log CFU cm^{-2} reduction) was observed with photoactivated Ber and Ber–Gen combination, while photoactivated Gen reduced culturability by ≈5 log CFU cm^{-2} ($P < 0.05$). Despite these pronounced effects, culturability recovery was observed within 72 h for both photoactivated and non-photoactivated Ber and Gen alone. In contrast, the photoactivated Ber–Gen combination maintained its partial inhibition and limited regrowth to 7 log CFU cm^{-2} compared to controls (≈8 log CFU cm^{-2}, $P < 0.05$).

The biomass results confirmed these observations and showed that after 24 h, neither Ber nor Gen alone, without photoactivation, caused a significant decrease ($P > 0.05$), while the combination reduced biomass by ≈30% (Fig. 3C, $P < 0.05$). In contrast, the photoactivated Ber and Ber–Gen resulted in a significant biomass reduction of ≈40–50% ($P < 0.05$). However, biomass recovered totally within 72 h with photoactivated and non-photoactivated Ber and Gen alone, while a reduction of ≈20% was maintained with photoactivated Ber–Gen combination ($P < 0.05$). In terms of metabolic activity, after 24 h, non-photoactivated Gen alone had no significant effect ($P > 0.05$), while non-photoactivated Ber and Ber–Gen reduced metabolic activity by 40% (Fig. 3D, $P < 0.05$). Photoactivated Ber further reduced metabolic activity by ≈60% ($P < 0.05$), and the photoactivated Ber–Gen combination achieved the

This journal is © The Royal Society of Chemistry 2026

Open Access Article. Published on 07 April 2026. Downloaded on 4/8/2026 2:33:27 PM.
This article is licensed under a Creative Commons Attribution 3.0 Unported Licence.

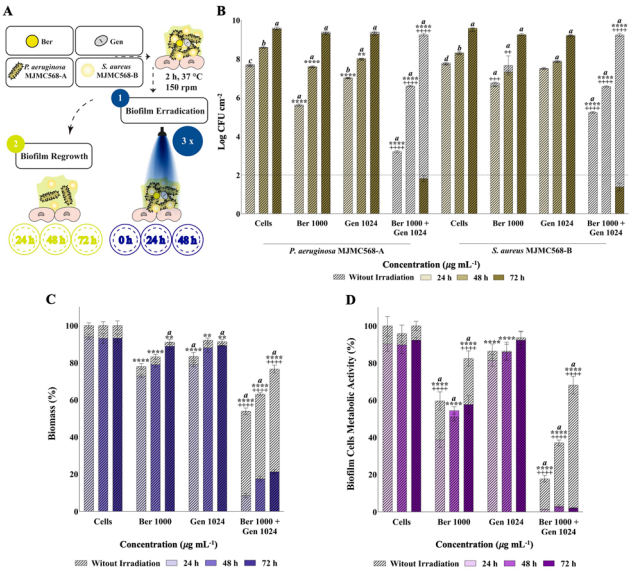

Fig. 5 Eradication of pre-formed dual-species *P. aeruginosa* MJMC568-A and *S. aureus* MJMC568-B biofilms with Ber, Gen, and their combination after three irradiation cycle. (A) Schematic representation of the experimental workflow: pre-formed dual-species biofilms were exposed to Ber, Gen, or Ber–Gen combination for 2 h at 37 °C under agitation (150 rpm), followed by blue light irradiation (420 nm, 30 mW cm^{-2}, 18 J cm^{-2}) during 10 min. Regrowth was assessed over 72 h by evaluating the culturability of *P. aeruginosa* MJMC568-A and *S. aureus* MJMC568-B, expressed as log CFU cm^{-2} (B), total biomass (C), and metabolic activity (D). Data are presented as mean ± SDs for two independent experiments with at least three replicates. Statistical analyses were performed between irradiated and non-irradiated groups (represented by the +), relative to untreated biofilm controls (represented by *), and between time points (24, 48, and 72 h), with significant differences indicated by the letters above the bars.

strongest inhibition (≈70%, $P < 0.05$). Despite almost total recovery over 72 h, both photoactivated and non-photoactivated Ber and Ber–Gen maintained ≈20% ($P < 0.05$) inhibition of metabolic activity, while Gen remained ineffective ($P > 0.05$).

The application of two consecutive cycles of blue light irradiation further enhanced the activity of the Ber–Gen combination against dual-species *P. aeruginosa* MJMC568-A and *S. aureus* MJMC568-B biofilms compared to a single irradiation cycle. After 24 h, non-photoactivated Ber or Gen alone reduced culturability by approximately 1 log CFU cm^{-2} in both species (Fig. 4B, $P < 0.05$). The non-photoactivated Ber–Gen combination caused a greater reduction of ≈5 log CFU cm^{-2} for both strains ($P < 0.05$). Blue light photoactivated Ber–Gen markedly potentiated these effects, leading to a reduction of ≈6 log CFU cm^{-2} for *P. aeruginosa* MJMC568-A and complete eradication (≈8 log CFU cm^{-2} reduction) for *S. aureus* MJMC568-B ($P < 0.05$).

Notably, unlike the regrowth observed after a single irradiation cycle, culturability remained strongly suppressed over 72 h, with the photoactivated Ber–Gen combination maintaining a reduction of ≈4 log CFU cm^{-2} for both strains ($P < 0.05$). Biomass results were consistent with these observations (Fig. 4C), where after 24 h, non-photoactivated Ber and Gen alone showed no significant effect ($P > 0.05$), while their combination reduced biomass by ≈50% ($P < 0.05$). Photoactivation significantly enhanced this effect, with Ber and Ber–Gen combination reducing biomass by ≈30% and ≈70% ($P < 0.05$), respectively. Notably, in contrast to the near-complete biomass recovery observed after a single cycle, two irradiation cycles sustained a significant biomass reduction of ≈50% with photoactivated Ber–Gen after 72 h ($P < 0.05$). Similarly, metabolic activity results (Fig. 4D) confirmed these findings, where after 24 h, non-photoactivated Gen alone was ineffective ($P > 0.05$), whereas Ber and Ber–Gen reduced activity by ≈30–40% ($P < 0.05$). Photoactivated Ber inhibited metabolic activity by ≈70%, while the photoactivated Ber–Gen combination achieved ≈80% inhibition ($P < 0.05$). Unlike the quick recovery observed after a single cycle, two irradiation cycles significantly delayed regrowth, with photoactivated Ber–Gen maintaining ≈30% inhibition of metabolic activity after 72 h ($P < 0.05$).

With the application of three consecutive cycles of blue light irradiation, the activity of the Ber–Gen combination against dual-species *P. aeruginosa* MJMC568-A and *S. aureus* MJMC568-B biofilms was markedly improved. After 24 h, non-photoactivated Ber or Gen alone reduced culturability by ≈1–2 log CFU cm^{-2} for *P. aeruginosa* MJMC568-A and ≈1 log CFU cm^{-2} for *S. aureus* MJMC568-B (Fig. 5B, $P < 0.05$). The non-photoactivated Ber–Gen combination produced a stronger reduction of ≈5 log CFU cm^{-2} for *P. aeruginosa* MJMC568-A and ≈3 log CFU cm^{-2} for *S. aureus* MJMC568-B ($P < 0.05$). Blue light markedly potentiated these effects, leading to complete eradication of both species with photoactivated Ber–Gen (≈8 log CFU cm^{-2} reduction, $P < 0.05$) after 24 h.

Notably, culturability remained strongly suppressed, with the photoactivated Ber–Gen combination sustaining complete eradication for 48 h and maintaining levels below the detection threshold (<2 log CFU cm^{-2}) after 72 h ($P < 0.05$). Biomass results were in agreement (Fig. 5C), showing that after 24 h, treatment with Ber or Gen alone, whether photoactivated or not, did not significantly reduce biofilm biomass ($P > 0.05$). In contrast, non-photoactivated Ber–Gen reduced biomass by ≈40%, while photoactivated Ber–Gen achieved a reduction of ≈90% ($P < 0.05$). Remarkably, after three irradiation cycles with Ber–Gen, biomass remained suppressed by ≈80% at 72 h, demonstrating sustained antibiofilm activity. Metabolic activity results (Fig. 5D) further supported these observations, where after 24 h, both photoactivated and non-photoactivated Gen were ineffective ($P > 0.05$), whereas non-photoactivated Ber and Ber–Gen reduced metabolic activity by ≈30% and ≈80%, respectively ($P < 0.05$). Photoactivated Ber inhibited metabolic activity by ≈60%, while photoactivated Ber–Gen achieved > 90% inhibition ($P < 0.05$). Crucially, in contrast to the recovery observed after one or two cycles, three irradiation cycles almost completely prevented regrowth, with photoactivated Ber–Gen maintaining > 90% inhibition of metabolic activity even after 72 h ($P < 0.05$). Overall, three irradiation cycles outperformed in all tests, demonstrating that repeated application of aPDI increases its efficacy against dual-species biofilms. Therefore, the three-cycle regimen was chosen for all subsequent

Open Access Article. Published on 07 April 2026. Downloaded on 4/8/2026 2:33:27 PM.
This article is licensed under a Creative Commons Attribution 3.0 Unported Licence.

tests.3.3 3.3 Antibiofilm mode of action of Ber–Gen combination after three irradiation cycles

To further clarify the mechanism of Ber–Gen after three irradiation cycles, its effects on intracellular ROS generation, biofilm architecture, extracellular matrix components (proteins, polysaccharides, and eDNA), and cell membrane integrity were examined (Fig. 6–8).

ROS quantification revealed that untreated biofilms maintained basal ROS levels throughout the three irradiation cycles, with only minor variations (Fig. 6B). In contrast, Ber–Gen significantly enhanced ROS generation, and this effect was more pronounced under photoactivation. After the first irradiation cycle, ROS levels in photoactivated Ber–Gen-treated biofilms reached approximately 200% relative to untreated controls, comparable to the positive control with 3% H_2O_2 (approximately 220%), while the non-photoactivated counterpart remained limited to approximately 120% ($P < 0.05$). Following the second irradiation cycle, ROS accumulation decreased slightly to ≈180% for photoactivated Ber–Gen, whereas the non-photoactivated one remained unchanged at ≈120% ($P < 0.05$). After the third cycle, ROS production further declined to ≈150% in photoactivated Ber–Gen-treated biofilms, approaching the levels observed with the non-photoactivated treatment (≈120%, $P < 0.05$). In contrast to the photoactivated Ber–Gen combination, both photoactivated and non-photoactivated H_2O_2 maintained its activity over the three irradiation cycles (≈220%, $P < 0.05$). Although the signal declined over successive irradiation cycles, this drop largely reflected the gradual loss of viable cells. Even with the reduction in cell number, photoactivated Ber–Gen still produced a marked increase in oxidative stress compared with untreated and non-photoactivated samples.

To determine whether this increase in oxidative stress translated into biofilm structural damage, the biofilm architecture was examined. The OCT analysis (Fig. 6C and D) confirmed the disruptive impact of treatment on biofilm architecture. Untreated biofilms exhibited thick and heterogeneous structures, with a maximum thickness of ≈250 μm, an average thickness of ≈50 μm, and a surface roughness of ≈35. Non-photoactivated Ber–Gen treatment significantly reduced these parameters to ≈150 μm (maximum thickness), ≈20 μm (average thickness), and ≈10 (roughness, $P < 0.05$). The strongest effects were observed with photoactivated Ber–Gen, which reduced maximum thickness to ≈40 μm, average thickness to ≈15 μm, and almost completely reduced roughness (1, $P < 0.05$). 2D-OCT inspections (Fig. 6C) illustrated these effects, showing compact and voluminous structures in untreated controls, partial collapse with non-photoactivated Ber–Gen, and almost complete disruption of the biofilm after photoactivated Ber–Gen treatment. Overall, the results demonstrate that Ber–Gen strongly disrupts the extracellular biofilm matrix and profoundly destabilizes biofilm 3D architecture, with photoactivation amplifying these effects to near-complete collapse.

Regarding the extracellular matrix, CLSM images (Fig. 7A) showed that untreated dual-species biofilms, with or without irradiation, displayed a dense protein- and eDNA-rich matrix.

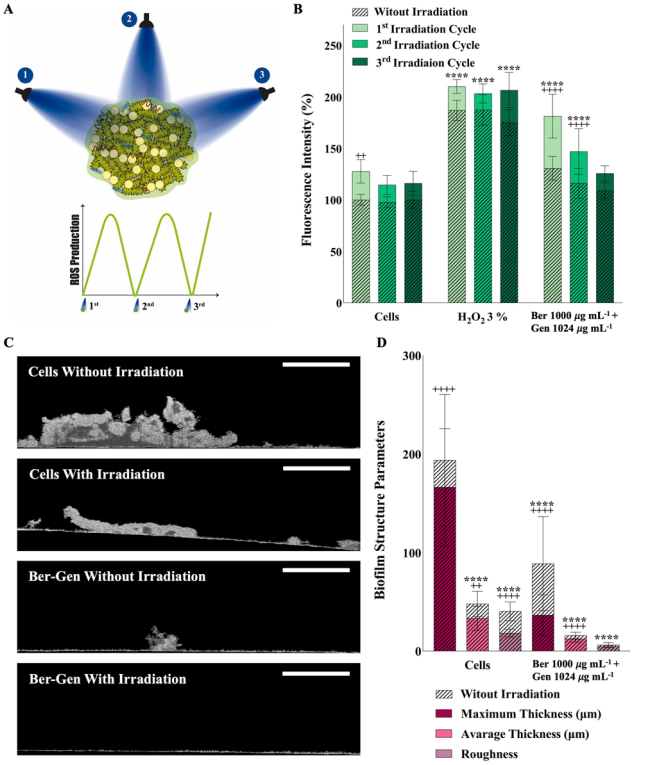

Fig. 6 ROS production and characterization of the architecture of dual-species *P. aeruginosa* MJMC568-A and *S. aureus* MJMC568-B biofilms after treatment with the Ber–Gen combination under multiple irradiation cycles. (A) Schematic overview of the experimental design: biofilms were treated once daily with Ber–Gen combination followed by 10 min blue light exposure (420 nm, 30 mW cm^{-2}, 18 J cm^{-2}), and ROS production was assessed immediately after each irradiation. (B) DCF-DA fluorescence intensity corresponding to ROS production levels in dual-species biofilms. (C) Representative 2D-OCT reconstructions illustrating the effects of treatments on biofilm architecture. The scale bar corresponds to 250 μm, and the visualisation field was 3.66 × 2.98 mm^3 in the X–Z section, which corresponds to 1024 pixels × 1024 pixels. (D) Measurements of specific biofilm structure parameters at the mesoscale, including maximum thickness, average thickness, and surface roughness, obtained based on 2D-OCT image processing. Data are presented as mean ± SD from two independent experiments with at least three replicates. Statistical analyses were performed between irradiated and non-irradiated groups (+) and relative to untreated biofilm controls (*).

In contrast, treatment with Ber–Gen markedly reduced extracellular proteins and eDNA, with the effect being more pronounced under photoactivation.

Quantitative analysis of EPS (Fig. 7B) confirmed these findings, where extracellular protein levels decreased from ≈70 μg mL^{-1} to ≈50 μg mL^{-1} after non-photoactivated Ber–Gen and to ≈20 μg mL^{-1} after photoactivated Ber–Gen ($P < 0.05$). Similarly, extracellular polysaccharide content decreased from ≈25 μg mL^{-1} in untreated biofilms to ≈15 μg mL^{-1} with non-photoactivated Ber–Gen and to ≈10 μg mL^{-1} with photoactivated Ber–Gen ($P < 0.05$). Fluorimetric quantification of eDNA (Fig. 7C) further supported these results, showing a significant decrease compared to untreated controls, resulting in a reduction of ≈50% with photoactivated Ber–Gen and ≈30% with the non-photoactivated condition ($P < 0.05$).

This journal is © The Royal Society of Chemistry 2026

Open Access Article. Published on 07 April 2026. Downloaded on 4/8/2026 2:33:27 PM.
This article is licensed under a Creative Commons Attribution 3.0 Unported Licence.

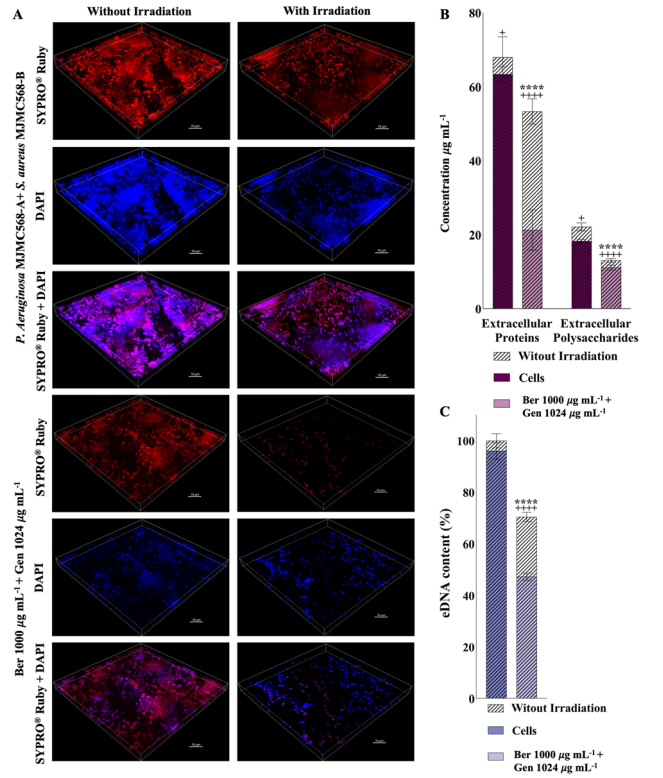

Fig. 7 Characterization of the extracellular matrix of dual-species *P. aeruginosa* MJMC568-A and *S. aureus* MJMC568-B biofilms after treatment with the Ber–Gen combination under multiple irradiation cycles. (A) Representative 3D CLSM images of dual-species *P. aeruginosa* MJMC568-A and *S. aureus* MJMC568-B biofilms stained with SYPRO® Ruby for extracellular proteins (red) and DAPI for eDNA (blue); scale bar = 10 μm. (B) Quantification of extracellular proteins by the Bradford assay and polysaccharides by the phenol–sulfuric acid method. (C) Quantification of eDNA content by DAPI fluorescence. Data are presented as mean ± SD from two independent experiments with at least three replicates. Statistical analyses were performed between irradiated and non-irradiated groups (+) and relative to untreated biofilm controls (*).

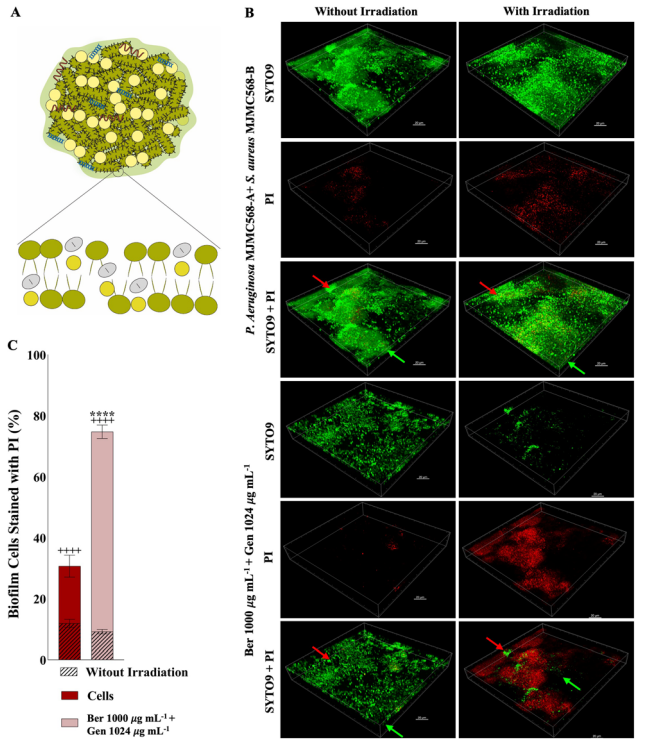

Fig. 8 Characterization of the spatial organization and membrane integrity of cells within dual-species *P. aeruginosa* MJMC568-A and *S. aureus* MJMC568-B biofilms after treatment with Ber–Gen combination under multiple irradiation cycles. (A) Schematic representation of the dual-species biofilm showing the spatial organisation of *P. aeruginosa* and *S. aureus* and the membrane integrity. (B) Representative 3D-CLSM images of dual-species *P. aeruginosa* MJMC568-A and *S. aureus* MJMC568-B biofilms, illustrating the spatial distribution of intact cells, stained with SYTO 9 (green) and membrane-compromised cells, stained with PI (red) within biofilm; red arrows mark regions enriched in *S. aureus* MJMC568-B, while green arrows point to areas dominated by *P. aeruginosa* MJMC568-A (scale bar = 20 μm). (C) Membrane integrity of dual-species biofilms quantitatively evaluated by PI uptake through flow cytometry. Data are presented as mean ± SD from two independent experiments with at least three replicates. Statistical analyses were performed between irradiated and non-irradiated groups (+) and relative to untreated biofilm controls (*).

The structural disruption was also evident in CLSM images showing the 3D distribution of cells within biofilm (Fig. 8B). Untreated dual-species biofilms, with or without irradiation, exhibited a dense, 3D architecture organised into aggregates. In these consortia, *P. aeruginosa* predominated in the basal layers (green arrows), forming compact structures, while *S. aureus* was preferentially located in the superficial areas (red arrows), presenting a more dispersed arrangement. Ber–Gen treatment caused marked disorganisation of the biofilm structure, resulting in loss of confluence and a clear reduction in diffuse green zones, consistent with the eDNA quantification results. Regarding to photoactivated Ber–Gen, there was an almost complete collapse of the biofilm, with only isolated *S. aureus* and *P. aeruginosa* cells remaining.

In terms of membrane integrity, untreated dual-species biofilms display continuous green fluorescence and slight zones of red fluorescence, indicating high membrane integrity and preserved architecture. In contrast, non-photoactivated Ber–Gen caused partial thinning of the biofilm structure, with dispersed PI-stained cells. Under photoactivation, however, the biofilm exhibited a pronounced collapse of its 3D architecture, with large discontinuous areas, loss of compactness, and extensive red fluorescence, indicating widespread membrane damage. Quantitative analysis (Fig. 8C) confirmed these observations, where blue light alone disrupted membrane integrity, increasing PI-stained cells from $\approx$15% in untreated controls to $\approx$35% ($P < 0.05$). A similar effect was observed for Ber–Gen, where the photoactivated treatment resulted in $\approx$80% of cells stained with PI, consistent with extensive structural disruption, while the non-photoactivated counterpart accounted for only $\approx$15% ($P < 0.05$).

4. Discussion

The present study aimed to evaluate, for the first time, the efficacy of aPDI using Ber–Gen combination against dual-

Open Access Article. Published on 07 April 2026. Downloaded on 4/8/2026 2:33:27 PM. This article is licensed under a Creative Commons Attribution 3.0 Unported Licence.

species *P. aeruginosa* and *S. aureus* biofilms isolated from a DFU, providing a more clinically relevant approach. In particular, Gonçalves *et al.*[17] characterised the antibiotic susceptibility profile of these planktonic strains and found that both displayed a multidrug-resistant phenotype, including resistance to Gen. Given this profile, as a first step, the MBIC and MBEC of Ber, Gen, and their combination were assessed against preformed dual-species biofilms. The Ber–Gen combination exhibited synergistic effects at the MBIC level but did not significantly reduce MBEC values, suggesting that it can affect biofilm growth but is unable to achieve complete eradication. The improved effect at the MBIC level can be attributed to the multi-target nature of the Ber–Gen combination, which simultaneously interferes with distinct cellular metabolic pathways and decreases the likelihood of bacterial adaptation. Although no studies have previously evaluated this combination for the eradication of pre-formed dual-species biofilms, the findings of the present study are consistent with those of Gonçalves *et al.*,[17] who demonstrated the synergistic activity of this combination against planktonic *S. aureus* MJMC568-B. This interpretation is further supported by growth curve analysis (Gompertz model), in which Ber and Gen individually reduced A_{max} and rendered μ_m negative, whereas their combination produced the most pronounced inhibition of growth capacity and almost abolished the lag phase. These findings demonstrate that the multi-target approach confers inherent advantages against mixed biofilms, although complete eradication still requires complementary strategies such as aPDI.

Photoactivation with blue light markedly potentiated the antibiofilm activity of the Ber–Gen combination. A single irradiation cycle reduced culturability, biomass, and metabolic activity (achieving a total eradication of *S. aureus* and a strong reduction of *P. aeruginosa*). This synergistic effect was also reported by Li *et al.*,[42] who investigated the activity of indocyanine green combined with EDTA and either vancomycin or amikacin under near-infrared (NIR) irradiation against MRSA or multidrug-resistant *P. aeruginosa* biofilms isolated from DFUs. The authors observed marked synergy with the triple combination (indocyanine green, EDTA, and vancomycin or amikacin with NIR light), achieving up to a 90% reduction in biofilm cells. The enhanced synergy was attributed to increased antibiotic uptake facilitated by oxidative damage induced by aPDI. However, the study did not investigate the effect over time, leaving the question of sustained biofilm regrowth unresolved. Indeed, there is a significant knowledge gap regarding strategies to enhance aPDI with antibiotics against biofilms associated with DFU infections, especially in the context of polymicrobial communities.

Overall, the results of the present study indicate that repetition of light exposure, together with the combined activity of Ber–Gen, is a critical parameter for overcoming the regrowth of dual-species biofilms, rather than simply increasing a single-dose treatment. This can be explained by the reduced capacity of the biofilm to adapt when exposed to multiple and sequential stimuli. In contrast, when agents are applied individually, bacteria are more likely to adapt and withstand their effects than under a multi-target approach.[20,43] In particular, this effect was observed in *S. aureus*, where the application of Ber and Gen alone, even under photoactivation, leads to an apparent tolerance during the three irradiation cycles. Although Ber and Gen showed significant antibiofilm effects after the first application, their activity markedly decreased during subsequent cycles. This adaptive effect of *S. aureus* may be related to the formation of small colony variants (SCVs), a phenotype frequently described in dual-species *P. aeruginosa* and *S. aureus* biofilms.[44] The adaptation is driven by 2-heptyl-4-hydroxyquinoline *N*-oxide (HQNO), an exoproduct of the *Pseudomonas* Quinolone Signal (PQS) quorum sensing system.[44] HQNO interferes with the electron transport chain of *S. aureus*, particularly the cytochrome bc1 complex, making aerobic respiration impossible and forcing cells to switch to fermentative metabolism.[44] As a result, *S. aureus* develops slow-growing SCVs, characterised by reduced metabolic activity, increased antibiotic tolerance, and a higher ability to persist within biofilms.[45] This alteration provides a plausible explanation for the limited cumulative effect observed after repeated treatments, as SCVs are less susceptible to antimicrobials and oxidative damage, thus supporting *S. aureus* survival.

In contrast, throughout the repeated applications, *P. aeruginosa* consistently proved to be more recalcitrant to treatment from the first exposure. This higher recalcitrance can be attributed to the structural features of Gram-negative pathogens, particularly concerning antimicrobial uptake.[46] *P. aeruginosa* possesses some characteristics that make it markedly more resistant to antimicrobials than *S. aureus*. While *S. aureus* is a Gram-positive bacterium with a thick peptidoglycan cell wall that remains relatively permeable to many hydrophilic antimicrobials, *P. aeruginosa* is Gram-negative, with an outer membrane that provides an additional physical barrier.[10,20] This membrane is enriched in lipopolysaccharides, which reduce permeability to antimicrobials and hinder their penetration.[47] Beyond this intrinsic barrier, *P. aeruginosa* is also known for its remarkable ability to withstand oxidative stress by upregulating antioxidant enzymes (*e.g.*, catalases, peroxidases, superoxide dismutases) and redox-balancing systems that limit ROS accumulation.[26] Under stress, *P. aeruginosa* further reinforces its defences by increasing exopolysaccharide production, activating efflux pumps, and releasing signaling molecules, such as HQNO.[48] Therefore, the initial stress imposed on *P. aeruginosa* not only selects for more resistant subpopulations of this bacterium but also indirectly promotes the persistence of *S. aureus* during subsequent treatments. These interactions may be further exacerbated in diabetic wound environments. Hyperglycaemic conditions, characteristic of DFUs, increase nutrient availability in the wound environment, promoting microbial proliferation and impairing host immunity. It also favours the accumulation of advanced glycation end products (AGEs), which enhance biofilm formation. In *S. aureus*, AGEs are associated with activation of stress-response regulators and increased eDNA production, while in *P. aeruginosa*, hyperglycaemia stimulates cyclic di-GMP signalling, inducing *pel* and *psl* expression and extracellular polysaccharide synthesis, which stabilise biofilms.

 This journal is © The Royal Society of Chemistry 2026

Open Access Article. Published on 07 April 2026. Downloaded on 4/8/2026 2:33:27 PM. This article is licensed under a Creative Commons Attribution 3.0 Unported Licence.

While the adaptive stress response of *P. aeruginosa* plays a central role in increasing *S. aureus* tolerance, it should also be recognised that both species can create their own adaptive responses.[10] Therefore, the recalcitrance of mixed biofilms should be considered the result of a bidirectional and dynamic adaptation, rather than the isolated response of a single species.[49]

Given this dynamic and cooperative adaptation within dual-species biofilms, it is crucial to clarify how the Ber–Gen combination, especially under photoactivation, can overcome such defence mechanisms. Indeed, the dense extracellular matrix of biofilms is a major barrier to compound uptake and therefore limits their antibacterial activity.[46] This is particularly evident in dual-species *P. aeruginosa* and *S. aureus* biofilms, which possess a more robust extracellular matrix, enriched in protein, polysaccharides, and eDNA, and display greater antibiotic tolerance than single-species biofilms.[50] These dual-species biofilms are denser, thicker, and structurally more heterogeneous, largely due to the combination and complementarity of exopolymers produced by both species.[51] *P. aeruginosa* synthesises polysaccharides such as alginate, Pel, and Psl, which provide cohesion and structural stability, whereas *S. aureus* contributes with intercellular adhesion polysaccharides, proteins, and eDNA, thereby increasing matrix density.[52,53] Beyond this accumulation of matrix components, interspecies metabolic and molecular interactions also play a pivotal role. In particular, while HQNO modulates *S. aureus* metabolism and promotes the emergence of SCVs, *S. aureus* can also increase *P. aeruginosa* virulence, increasing the levels of LasB elastase, rhamnolipids, exotoxins, and phenazines.[54] Together, these consortia create pronounced gradients of oxygen and nutrients that support the coexistence of metabolically distinct subpopulations and further increase biofilm heterogeneity.[10] In line with this spatial and metabolic stratification, the results of the present study show that *P. aeruginosa* predominantly occupies the basal layer, while *S. aureus* is located near the biofilm surface, consistent with the distribution described by Pouget *et al.*[55] The authors investigated the spatial organisation of dual-species *P. aeruginosa* and *S. aureus* biofilms isolated from a patient with DFU. They observed that *S. aureus* aggregates were found near the wound surface, while *P. aeruginosa* was located deeper in the wound bed.

Although dual-species biofilm matrices represent a strong protective barrier, both photoactivated and non-photoactivated Ber–Gen treatments demonstrated a clear ability to disrupt their 3D structure. This structural collapse was accompanied by significant reductions in extracellular proteins, polysaccharides, and eDNA, ultimately resulting in thinner and less cohesive biofilms. These findings are consistent with previous reports showing that Ber targets *P. aeruginosa* and *S. aureus* biofilm structure, even in the absence of photoactivation. Liu *et al.*,[56] demonstrated that Ber downregulates *pslA* and *pelA*, two key genes responsible for exopolysaccharide synthesis in *P. aeruginosa* biofilms, thereby weakening matrix cohesion. Similarly, Chu *et al.*,[57] showed that Ber inhibits the assembly of amyloid fibrils in MRSA by binding to phenol-soluble modulins (PSMs), disrupting hydrophobic interactions with residues such as Phe19 in PSMα2. Since PSM-derived amyloids are crucial for the mechanical stability of the *S. aureus* biofilm matrix, their disruption by Ber leads to a loss of matrix integrity and reduced tolerance. The interaction of Ber with the EPS can be explained by its positive charge, conferred by the quaternary ammonium group, which enables it to associate with negatively charged EPS components.[58] Similarly, Gen contains cationic groups that allow electrostatic interaction with the anionic components of EPS.[59] In addition, our data strongly suggests that the Ber–Gen combination may also interfere with eDNA within dual-species biofilms. Although, to the best of the authors' knowledge, no study has directly evaluated the action of Ber or Gen on eDNA in *P. aeruginosa* or *S. aureus* biofilms, their chemical structure provides a strong rationale. The Ber's planar π-conjugated system and a quaternary ammonium group together enable DNA intercalation *via* π–π stacking as well as electrostatic interactions with the negatively charged phosphate backbone.[60] This mechanism may explain the strong reduction of eDNA observed with the non-photoactivated Ber–Gen combination in our study, consistent with earlier evidence from Gonçalves *et al.*,[20] who showed that Ber–Gen interferes with DNA stability in *S. aureus* MJMC568-B in the planktonic state.

Beyond biofilm structure disruption, Ber's quaternary ammonium group also could interact electrostatically with bacterial membrane phosphates, promoting depolarisation and destabilisation of membrane integrity.[61] Meanwhile, its π-conjugated scaffold favours electron delocalisation, conferring redox-active properties that allow it to accept and donate electrons in intracellular redox cycles.[61] These properties enhance oxidative stress, explaining why non-photoactivated Ber–Gen already induced ROS production. On the other hand, Gen primarily targets the 30S ribosomal subunit, irreversibly disrupting protein synthesis and promoting mistranslation, which has been associated with oxidative stress.[59] However, Gen's hydroxyl-rich structure has been proposed to promote hydroxyl radical formation *via* electron transfer, contributing further to ROS accumulation.[20] Together, these mechanisms explain the ability of non-photoactivated Ber–Gen to impair membrane integrity and trigger ROS production in dual-species biofilms. Similarly to DNA damage, the ROS results for non-photoactivated Ber–Gen are consistent with those obtained by Gonçalves *et al.*,[20] who observed that the Ber–Gen combination leads to strong ROS production even without blue light activation against planktonic *S. aureus* MJMC568-B.

Notably, photoactivation with blue light introduces additional and complementary mechanisms of action that amplify these effects. Blue light irradiation generates ROS within the biofilm matrix, which oxidise extracellular proteins, polysaccharides, and eDNA, thereby destabilising the structural scaffold.[62] This was observed in the present study, where blue light alone significantly reduced matrix components. At the cellular level, ROS promotes lipid peroxidation, leading to increased membrane permeability and loss of integrity, while also damaging intracellular macromolecules such as DNA and proteins.[63] Indeed, although blue light alone is a potent ROS inducer, our results demonstrated that photoactivation of the Ber–Gen combination markedly enhanced oxidative stress

Open Access Article. Published on 07 April 2026. Downloaded on 4/8/2026 2:33:27 PM.
This article is licensed under a Creative Commons Attribution 3.0 Unported Licence.

within the biofilm. The synergistic increase in ROS production can be attributed to the interplay between light-induced ROS, Ber's redox cycling properties, and Gen's capacity to stimulate radical formation. ROS play a central role in this combined photodynamic effect, as the oxidative stress, which generates damage to the biofilm matrix and bacterial membranes, destabilizes the biofilm structure and enhances Ber–Gen activity. Importantly, this triple contribution to oxidative stress resulted in pronounced loss of membrane integrity and a sharp increase in PI-stained cells, which was far more significant than under non-photoactivated conditions. These effects indicate that ROS-mediated oxidative damage, combined with the membrane-interacting properties of Ber, contributes to the loss of bacterial membrane integrity and enhances the antibiofilm activity of the Ber–Gen combination. Although intracellular antibiotic uptake was not directly assessed in this study, this ROS-mediated membrane destabilisation may facilitate Gen penetration into bacterial cells, potentially helping overcome the intrinsic tolerance of antibiotic-resistant biofilm cells. Taken together, these results suggest that the simultaneous action of Ber, Gen, and blue light not only disrupts biofilm structure but also overwhelms bacterial antioxidant defences, leading to cell death and preventing regrowth.

Overall, the present results show that multiple irradiation cycles using the Ber–Gen combination represent a promising strategy for overcoming the intrinsic recalcitrance of dual-species *P. aeruginosa* and *S. aureus* biofilms isolated from DFUs. This multi-target approach interferes with biofilm integrity by reducing biomass, metabolic activity, and culturability, while disrupting the extracellular matrix and simultaneously affecting several cellular targets, including bacterial membranes, DNA, and intracellular redox balance, ultimately enhancing Gen activity. The combined action of Ber, Gen, and blue light not only kills active bacteria but also could interfere with adaptive phenotypes such as SCVs, whose low metabolic activity tends to reduce the efficacy of conventional antibiotics. In particular, the enhanced antibiofilm activity against biofilm-forming DFU isolates suggests that it may partially overcome the resistance typically associated with Gen in biofilms. Although biofilm regrowth was strongly suppressed, and culturability remained below the detection limit after 72 h, increasing the number of irradiation cycles may further enhance this regrowth inhibition. In addition to decreasing the biofilm tolerance, extracellular matrix disruption is particularly relevant since it exposes bacterial cells to the host immune response, facilitating phagocytosis and access to antimicrobials, thus enhancing wound healing.[18] Furthermore, matrix destabilisation reduces biofilm thickness and cohesion, allowing blue light to penetrate and reach deeper layers. These processes contribute to both antimicrobial effect and wound healing, making photoactivation particularly relevant in chronic wounds such as DFUs, where tissue regeneration is compromised.

5. Conclusions

The results of the present study underscore, for the first time, the strong potential of blue light multiple irradiation cycles using Ber–Gen to treat dual-species *P. aeruginosa* and *S. aureus* biofilms associated with DFUs. While Ber–Gen proved to be a powerful synergistic combination capable of restoring the antibacterial activity of Gen, blue light photoactivation emerged as the key factor for the efficient eradication of preformed dual-species biofilms. Repeated irradiation cycles using the Ber–Gen combination not only enhanced biofilm eradication efficacy but also effectively prevented regrowth, sustaining the efficacy for up to 72 h. In particular, the multiple irradiation cycles using Ber–Gen acted as a powerful multi-target strategy, capable of strongly attacking dual-species biofilms. In addition to the strong disruption of biofilm structure by targeting extracellular proteins, polysaccharides, and eDNA, the present strategy demonstrated remarkable activity in compromising membrane integrity and increasing bacterial oxidative stress. Overall, these findings highlight the promising therapeutic alternative approach of blue light photoactivated Ber–Gen for managing persistent mixed *P. aeruginosa* and *S. aureus* biofilm-associated DFUs.

Despite the encouraging results, additional research would be beneficial to broaden and validate these observations. Although the blue light photoactivated Ber–Gen combination showed a strong antibiofilm effect, its cytotoxic effects on mammalian cells were not evaluated. As the present strategy relies on the generation of ROS, potential effects on host cells cannot be excluded. Therefore, future studies should investigate the biocompatibility of this approach using relevant skin cell models (such as co-cultures of fibroblasts and keratinocytes) and *in vivo* wound systems to better assess its therapeutic safety. Furthermore, assessing the effectiveness of photoactivated Ber–Gen combinations *in vivo* using diabetic ulcer models is crucial, as factors such as tissue hypoxia, local microbiome variability, exudate, and skin characteristics may impact both the efficacy of light and the diffusion of the compounds. Additionally, the variability among clinical isolates could influence the proposed strategy's effectiveness, given that the synergy between Ber and Gen is significantly affected by the concentration used, which can differ substantially from one strain to another. However, this strategy shows strong potential for clinical translation through photosensitive dressings capable of delivering local and repeatable doses directly at the wound site. Therefore, Ber–Gen-mediated aPDI emerges as a selective, locally applicable intervention that could complement standard care and effectively counteract the antibiotic recalcitrance of dual-species biofilm-associated infections.

Author contributions

Ariana S.C. Gonçalves: conceptualization, methodology, validation, formal analysis, investigation, writing – original draft; Miguel M. Leitão: methodology, investigation; Manuel Simões: resources, writing – review & editing, supervision, funding acquisition; Anabela Borges: conceptualization, resources, methodology, writing – review & editing, supervision, project administration, funding acquisition.

 This journal is © The Royal Society of Chemistry 2026

Open Access Article. Published on 07 April 2026. Downloaded on 4/8/2026 2:33:27 PM. This article is licensed under a Creative Commons Attribution 3.0 Unported Licence.

Conflicts of interest

There are no conflicts to declare.

Abbreviations

aPDI	Antimicrobial photodynamic inactivation;
PS	Photosensitiser
ROS	Reactive oxygen species
H_2O_2	Hydrogen peroxide
Ber	Berberine
Gen	Gentamicin
TSB	Tryptic soy broth
TSA	Tryptic soy agar
dH_2O	Distilled water
DMSO	Dimethyl sulfoxide
LED	Light-emitting diode device
OD	Optical density
CFU	Colony-forming units
NaCl	Saline soluction
MTC	Maximum tested concentration
CKB	Checkerboard
FICI	Fractional index
PI	Propidium iodide
MBIC	Minimum biofilm inhibitory concentration
MBEC	Minimum biofilm inhibitory concentration
MBEC	Minimum biofilm eradication concentration
OCT	Optical coherence tomography
BISCAP	Biofilm imaging and structure classification automatic processor
DCF-DA	2,7-Dichlorodihydrofluorescein diacetate
SDs	Standard deviations
EPS	Extracellular polymeric substances
eDNA	Extracellular DNA
CLSI	Clinical and laboratory standards institute
MRSA	Methicillin resistant *S. aureus*
2D	Two-dimensional
3D	Three-dimensional
CLSM	Confocal Laser Scanning Microscopy
PSMs	Phenol-soluble modulins
DFU	Diabetic foot ulcer
EPS	Extracellular polymeric substances
CV	Crystal violet
AB	Alamar blue
DAPI	′,6-diamidino-2-phenylindole
BSA	Bovine serum albumin
NIR	Near-infrared
EDTA	Ethylenediamine tetraacetate
SCVs	Small colony variants
HQNO	Heptyl-4-hydroxyquinoline *N*-oxide
PQS	Pseudomonas quinolone signal.

Data availability

Data will be made available on request.

Acknowledgements

This work was supported by: Project MultAntiBiofilm (ref. COMPETE2030-FEDER-00852000; N° 17121); and HCAI_Disinfect (ref. COMPETE2030-FEDER-00752300; N° 16360), co-funded by European Union through the Operational Programme Competitiveness Factors-COMPETE 2030, and by national funds through the Foundation for Science and Technology-FCT/MECI; Project InnovAntiBiofilm (ref. 101157363) financed by European Commission (Horizon-Widera 2023 - Acess-02/Horizon-CSA); and LEPABE, UID/00511/2025 (https://doi.org/10.54499/UID/00511/2025) e UID/PRR/00511/2025 (https://doi.org/10.54499/UID/PRR/00511/2025) e ALiCE, LA/P/0045/2020 (https://doi.org/10.54499/LA/P/0045/2020), funded by national funds through the FCT/MECI (Lisbon, Portugal). Ariana S.C. Gonçalves (reference: 2022.10913.BD and DOI: https://doi.org/10.54499/2022.10913.BD) and Miguel M. Leitão (reference: 2021.07145.BD and DOI: https://doi.org/10.54499/2021.07145.BD) acknowledge individual PhD fellowships from FCT. The data of this work was patented (PT 121240).

References

1 G. FrykbergRobert, *Adv. Wound Care*, 2015, **4**(9), 560–582.
2 A. Clinton and T. Carter, *Lab. Med.*, 2015, **46**, 277–284.
3 W. Alam, J. Hasson and M. Reed, *J. Am. Geriatr. Soc.*, 2021, **69**, 2327–2334.
4 R. Naganandini, *Indian J. Contin. Nurs. Educ.*, 2024, **25**, 128–132.
5 M. Vuorlaakso, J. Kiiski, T. Salonen, M. Karppelin, M. Helminen and I. Kaartinen, *Front. Surg.*, 2021, **8**, 655902.
6 D. G. Armstrong, T.-W. Tan, A. J. Boulton and S. A. Bus, *JAMA*, 2023, **330**, 62–75.
7 A. C. Afonso, D. Oliveira, M. J. Saavedra, A. Borges and M. Simões, *Int. J. Mol. Sci.*, 2021, **22**, 8278.
8 A. Malik, Z. Mohammad and J. Ahmad, *Diabetes Metab. Syndr.*, 2013, **7**, 101–107.
9 A. S. Gonçalves, M. M. Leitão, M. Simões and A. Borges, *Nat. Prod. Rep.*, 2023, **40**(3), 595–627.
10 R. Serra, R. Grande, L. Butrico, A. Rossi, U. F. Settimio, B. Caroleo, B. Amato, L. Gallelli and S. De Franciscis, *Expert Rev. Anti-Infect. Ther.*, 2015, **13**, 605–613.
11 S. DeLeon, A. Clinton, H. Fowler, J. Everett, A. R. Horswill and K. P. Rumbaugh, *Infect. Immun.*, 2014, **82**, 4718–4728.
12 T. Beaudoin, Y. C. W. Yau, P. J. Stapleton, Y. Gong, P. W. Wang, D. S. Guttman and V. Waters, *npj Biofilms Microbiomes*, 2017, **3**, 25.
13 P. K. Vestweber, J. Wächter, V. Planz, N. Jung and M. Windbergs, *PLoS One*, 2024, **19**, e0304491.
14 A. Clinton and T. Carter, *Adv. Wound Care*, 2015, **4**, 373–381.
15 P. R. Cavanagh, B. A. Lipsky, A. W. Bradbury and G. Botek, *Lancet*, 2005, **366**, 1725–1735.
16 M. Bayat, R. Albright, M. R. Hamblin and S. Chien, *J. Lasers Med. Sci.*, 2022, 13.
17 A. S. Gonçalves, M. M. Leitão, J. R. Fernandes, M. J. Saavedra, C. Pereira, M. Simões and A. Borges, *J. Photochem. Photobiol., B*, 2024, **258**, 112978.

Open Access Article. Published on 07 April 2026. Downloaded on 4/8/2026 2:33:27 PM. This article is licensed under a Creative Commons Attribution 3.0 Unported Licence.

18 T. P. Prado, F. C. Zanchetta, B. Barbieri, C. Aparecido, M. H. Melo Lima and E. P. Araujo, *Life*, 2023, **13**, 575.
19 A. Yoshida, H. Sasaki, T. Toyama, M. Araki, J. Fujioka, K. Tsukiyama, N. Hamada and F. Yoshino, *Sci. Rep.*, 2017, **7**, 5225.
20 A. S. Gonçalves, J. R. Fernandes, M. J. Saavedra, N. M. Guimarães, C. Pereira, M. Simões and A. Borges, *Photodiagn. Photodyn. Ther.*, 2025, 104514.
21 E. Polat and K. Kang, *Biomedicines*, 2021, **9**, 584.
22 V. Chander, J. Aswal, R. Dobhal and D. Uniyal, *J. Phytopharmacol.*, 2017, **6**, 53–58.
23 A. Gasmi, F. Asghar, S. Zafar, P. Oliinyk, O. Khavrona, R. Lysiuk, M. Peana, S. Piscopo, H. Antonyak and J. J. Pen, *Curr. Med. Chem.*, 2024, **31**, 1214–1234.
24 Y. Feng, C. C. Tonon, S. Ashraf and T. Hasan, *Adv. Drug Delivery Rev.*, 2021, **177**, 113941.
25 C. Hou, L. Zhang, L. Wang, S. Zhao, J. Nie, W. Zhang, X. Su, S. Tian and Y. Li, *Photodiagn. Photodyn. Ther.*, 2024, **48**, 104228.
26 W. S. da Cruz Nizer, V. Inkovskiy, Z. Versey, N. Strempel, E. Cassol and J. Overhage, *Pathogens*, 2021, **10**, 1187.
27 A. Wozniak and M. Grinholc, *Front. Microbiol.*, 2018, **9**, 930.
28 A. C. Afonso, I. B. Gomes, M. J. Saavedra, L. C. Simões and M. Simões, *Sci. Total Environ.*, 2023, **875**, 162646.
29 S. Fernandes, I. B. Gomes and M. Simões, *Food Res. Int.*, 2023, **167**, 112680.
30 A. F. Silva, A. Borges, C. F. Freitas, N. Hioka, J. M. G. Mikcha and M. Simões, *Molecules*, 2018, **23**, 2288.
31 A. Borges, L. C. Simões, M. J. Saavedra and M. Simões, *Int. Biodeterior. Biodegrad.*, 2014, **86**, 25–33.
32 M. M. Leitão, T. F. Vieira, S. F. Sousa, F. Borges, M. Simões and A. Borges, *Microb. Pathog.*, 2024, **191**, 106663.
33 M. M. Leitão, A. S. C. Gonçalves, S. F. Sousa, F. Borges, M. Simões and A. Borges, *Biomed. Pharmacother.*, 2025, **187**, 118090.
34 I. Gomes, M. Simões and L. C. Simões, *Sci. Total Environ.*, 2016, **565**, 40–48.
35 D. A. Narciso, A. Pereira, N. O. Dias, L. F. Melo and F. G. Martins, *Bioinformatics*, 2022, **38**, 1708–1715.
36 M. M. Ali Mohammed, A. H. Nerland, M. Al-Haroni and V. Bakken, *J. Oral Microbiol.*, 2013, **5**, 20015.
37 A. R. Pereira, I. B. Gomes, L. Santos and M. Simões, *J. Hazard. Mater.*, 2024, **480**, 136222.
38 M. Dubois, K. Gilles, J. Hamilton, P. Rebers and F. Smith, *Nature*, 1951, **168**, 167.
39 E. Harlow and D. Lane, *CSH protocols*, 2006, **2006**(6), pdb.prot4644.
40 B. Zatorska, M. Groger, D. Moser, M. Diab-Elschahawi, L. S. Lusignani and E. Presterl, *Clin. Orthop. Relat. Res.*, 2017, **475**, 2105–2113.
41 M. M. Leitão, A. S. Gonçalves, J. Moreira, C. Fernandes, F. Borges, M. Simões and A. Borges, *Eur. J. Med. Chem.*, 2024, 117163.
42 X. Li, W. Huang, X. Zheng, S. Chang, C. Liu, Q. Cheng and S. Zhu, *Photodiagn. Photodyn. Ther.*, 2019, **25**, 300–308.
43 M. M. Leitão, A. S. Gonçalves, F. Borges, M. Simões and A. Borges, *Pharmacol. Rev.*, 2025, 100038.
44 L. R. Hoffman, E. Déziel, D. A. d'Argenio, F. Lépine, J. Emerson, S. McNamara, R. L. Gibson, B. W. Ramsey and S. I. Miller, *Proc. Natl. Acad. Sci. U. S. A.*, 2006, **103**, 19890–19895.
45 G. Mitchell, D. L. Séguin, A.-E. Asselin, E. Déziel, A. M. Cantin, E. H. Frost, S. Michaud and F. Malouin, *BMC Microbiol.*, 2010, **10**, 33.
46 A. Borges, M. J. Saavedra and M. Simoes, *Curr. Med. Chem.*, 2015, **22**, 2590–2614.
47 T. Nakae, *Microbiol. Immunol.*, 1995, **39**, 221–229.
48 M. F. Moradali, S. Ghods and B. H. Rehm, *Front. Cell. Infect. Microbiol.*, 2017, **7**, 39.
49 I. Cavallo, F. Sivori, A. Mastrofrancesco, E. Abril, M. Pontone, E. G. Di Domenico and F. Pimpinelli, *Biology*, 2024, **13**, 109.
50 M. F. Hansen, D. Ronin, H. T. Kiesewalter, C. I. Amador and M. Burmølle, *Biofilm Matrix*, Springer, 2024, pp. 187–214.
51 T. Biswas, M. Ahmed and S. Mondal, *Microb. Pathog.*, 2024, **195**, 106866.
52 K. M. Colvin, *Extracellular polysaccharides in Pseudomonas aeruginosa*, University of Washington, 2012.
53 S. Rath, S. Fatma and S. Das, *Crit. Rev. Biochem. Mol. Biol.*, 2025, 1–32.
54 A. Hotterbeekx, S. Kumar-Singh, H. Goossens and S. Malhotra-Kumar, *Front. Cell. Infect. Microbiol.*, 2017, **7**, 106.
55 C. Pouget, C. Dunyach-Remy, C. Magnan, A. Pantel, A. Sotto and J.-P. Lavigne, *Int. J. Mol. Sci.*, 2022, **23**, 10761.
56 Q. Liu, Y. Tang, S. Jiang, X. Yu, H. Zhu, X. Xie and X. Ning, *Microb. Pathog.*, 2024, **193**, 106774.
57 M. Chu, M.-b Zhang, Y.-c Liu, J.-r Kang, Z.-y Chu, K.-l Yin, L.-y Ding, R. Ding, R.-x Xiao and Y.-n Yin, *Sci. Rep.*, 2016, **6**, 24748.
58 J. Jin, G. Hua, Z. Meng and P. Gao, *Chin. Herb. Med*, 2010, **3**, 27–35.
59 S. G. Sarre and F. E. Hahn, *Trans. N. Y. Acad. Sci.*, 1967, **29**, 575–578.
60 M. L. Birrento, *University of Wollongong*, 2017.
61 L. Peng, S. Kang, Z. Yin, R. Jia, X. Song, L. Li, Z. Li, Y. Zou, X. Liang, L. Li, C. He, G. Ye, L. Yin, F. Shi, C. Lv and B. Jing, *Int. J. Clin. Exp. Pathol.*, 2015, **8**, 5217–5223.
62 M. Gambino and F. Cappitelli, *Biofouling*, 2016, **32**(2), 167–178.
63 M. Fasnacht and N. Polacek, *Front. Mol. Biosci.*, 2021, **8**, 671037.

 This journal is © The Royal Society of Chemistry 2026